phys. stat. sol. (a) **134**, 567 (1992)

Subject classification: 73.40; 85; S7.11

Microelectronics Research Center, New Jersey Institute of Technology, Newark[1])

Electrical Properties of Ti/Au/SiO_2/InP Structures

By

M. PATEL and N. M. RAVINDRA

Experimental studies of the electrical properties of Ti/Au/SiO_2/InP structures are presented here. The metal–insulator–semiconductor (MIS) capacitors were fabricated with oxide thicknesses of 195, 420, and 610 nm, respectively, on n-type InP substrates, using rapid thermal chemical vapor deposition (RTCVD) techniques. The characterization techniques employed in these experiments were high frequency capacitance–voltage (C–U) and current–voltage (I–U). The electrical parameters obtained from the C–U and I–U measurements are discussed.

Es werden experimentelle Untersuchungen der elektrischen Eigenschaften von Ti/Au/SiO_2/InP-Strukturen mitgeteilt. Die MIS-Kondensatoren mit Oxyddicken von 195, 420 und 610 nm werden auf n-InP-Substraten mittels der RTCVD-Technik hergestellt. Zur Charakterisierung der Strukturen werden Hochfrequenz-C–U- und I–U-Messungen durchgeführt. Die aus diesen Kurven erhaltenen elektrischen Parameter werden diskutiert.

1. Introduction

At the present time, among the III–V compound semiconductors, GaAs and InP have taken the position of being the most technologically important materials. The technological importance of InP comes about because of its use in electronic and photonic devices such as solar cells, laser diodes, photo detectors, high speed MISFET digital circuits, and microwave power devices. The optimum band gap of InP makes it an ideal material for photovoltaic energy conversion. It has high radiation resistance, high carrier mobility, and low power dissipation [1 to 4]. Significant progress has been made in these areas but further work is needed to understand certain fundamental issues. In this study, electrical measurements were performed on MIS structures formed on InP substrates. The MIS structures are widely used as test structures to characterize a wide variety of semiconductor material and device properties.

2. Process Steps

In this study, MIS devices have been prepared on n-type InP substrates having a doping density of 2×10^{19} cm^{-3} sulfur atoms. The insulating oxide films were produced using RTCVD technique at pressure of 12.35×10^2 Pa with the substrate held at a temperature of 550 °C in an ambient of $O_2 : SiH_4 = 10 : 1$. 100 nm of Au followed by 300 nm of Ti were sputter-deposited on SiO_2/InP to form MIS structures. Oxide thickness of 195, 420, and 610 nm, respectively, were used as the insulator. The thickness of the oxides was obtained by changing the time in the RTCVD reactor corresponding to 25, 30, and 40 s, respectively, for sets of samples A, B, and C. The oxide thickness was measured using a Rudolph ellipsometer [5].

[1]) Newark, New Jersey 07102, USA.

3. Experimental Details

Electrical measurements were performed on all three sets of devices, A, B, and C. In order to measure capacitance as a function of gate bias in steady state, the $C-U$ technique was used [6]. $C-U$ technique is preferred because of its simplicity and the detailed information available about the electrical behavior of the device. In this technique, a small alternating voltage is superimposed on the gate of the MIS capacitor. When the gate bias is swept from negative to positive values for a p-type MIS capacitor, the surface conditions vary. The static current–voltage measurements have been used in the present work to study the current conduction mechanisms of thick SiO_2 films deposited on InP substrates.

4. Methodology

The $C-U$ analysis considers the data of physical constants and dimensions obtained from $C-U$ measurements. The analysis results into:

Area: The area, A, can be calculated from the measured C_{max} by the relation

$$C_{max} = C_{ox} = \varepsilon_0 \varepsilon_{ox} A / t_{ox} . \tag{1}$$

Flatband capacitance: The flatband voltage is the voltage at which the flatband capacitance occurs on the observed forward (depletion) $C-U$ curve. The flatband capacitance, C_{fbs} is given by

$$C_{fbs} = A \sqrt{\varepsilon_s q^2 N_b / kT} . \tag{2}$$

The measured capacitance at flatband, C_{fb} has C_{max} in series with C_{fbs} and hence

$$C_{fb}^{-1} = C_{fbs}^{-1} - C_{max}^{-1} . \tag{3}$$

Flatband voltage: The flatband voltage is the voltage at which the observed capacitance is equal to the theoretical flatband capacitance. The voltage is independent of area but the capacitance is dependent on the oxide thickness, its dielectric constant, and semiconductor doping.

Shift in flatband voltage may be due to one or more of the following causes:

1. mobile ions in the oxide (sodium etc.);
2. ions, electrons, or holels injected into the oxide;
3. fixed charges at the oxide–semiconductor interface [7].

Threshold voltage: The onset of inversion and the flow of current in the MIS occurs at the gate 'threshold' or 'turn-on' voltage and is given by

$$U_{th} = U_{fb} + 2\varphi_B + \left(\frac{t_{ox}}{\varepsilon_s}\right) \sqrt{2\varepsilon_s q N_b 2\varphi_B} , \tag{4}$$

where the barrier height, φ_B, is

$$\varphi_B = \left(\frac{kT}{q}\right) \ln \left(\frac{N_b}{n_i}\right) \tag{5}$$

and N_b the bulk carrier concentration.

Fixed oxide charges: For a given work function difference φ_{ms}, the initial charge concentration affecting the flatband voltage U_{fb} is

$$N_f = \left(\frac{\varepsilon_{ox}}{qt_{ox}}\right)(\varphi_{ms} - U_{fb}), \tag{6}$$

where the metal–semiconductor work function difference φ_{ms} is

$$\varphi_{ms} = \varphi_m - \left(\chi + \frac{E_g}{2q} - \varphi_B\right) = 0, \tag{7}$$

where χ is the electron affinity. The maximum depletion width W_{max} is given by

$$W_{max} = \sqrt{2\varepsilon_s\varphi_m/qN_b}, \tag{8}$$

where the metal work function φ_m is

$$\varphi_m = 2\varphi_b + \frac{kT}{q}\ln\left(\frac{2q\varphi_b}{kT}\right). \tag{9}$$

5. Results and Discussion

5.1 Current–voltage measurements

The static I–U measurements were performed using a Keithley 236/237 source measure unit (SMU). The capacitors were biased with a constant current to accelerate breakdown as discussed by Harari [8]. Basically, the technique consists of permitting a constant current into the capacitor with the voltage varying until the breakdown occurs. For thin oxides, the technique is non-destructive because the choice of constant current is limited by the actual Fowler-Nordheim tunneling (FNT) current component. This FNT component of the current is a function of the oxide thickness. During I–U measurements the contact to the counter electrode is made by means of a probe placed directly on top of the capacitor. Representative experimental I–U curves for samples A, B, and C are shown in Fig. 1. We can see from the experimental results that the applied voltage is not sufficient to cause breakdown. In these experiments, the current is kept as low as 1 μA to have self-healing (non-destructive) breakdown. But, as shown in Fig. 1, current compliance value of 1 μA is not reached though the applied voltage was as high as 100 V. This is because of the thick oxide.

5.2 Carrier transport in insulating films

In an ideal MIS diode, the conductance of the insulating film is assumed to be zero. Real insulators, however, show carrier conduction when the electric field or temperature is sufficiently high. Dielectric field in an insulator, under biasing conditions, is estimated by

$$E_i = E_s\frac{\varepsilon_s}{\varepsilon_i}, \tag{10}$$

where, E_i and E_s are the electric fields in the insulator and the semiconductor, respectively, and ε_1 and ε_s are the corresponding permittivities. Hence the electric field in the oxide is about three times larger than that in the InP. But, as the oxide thickness is high here, at

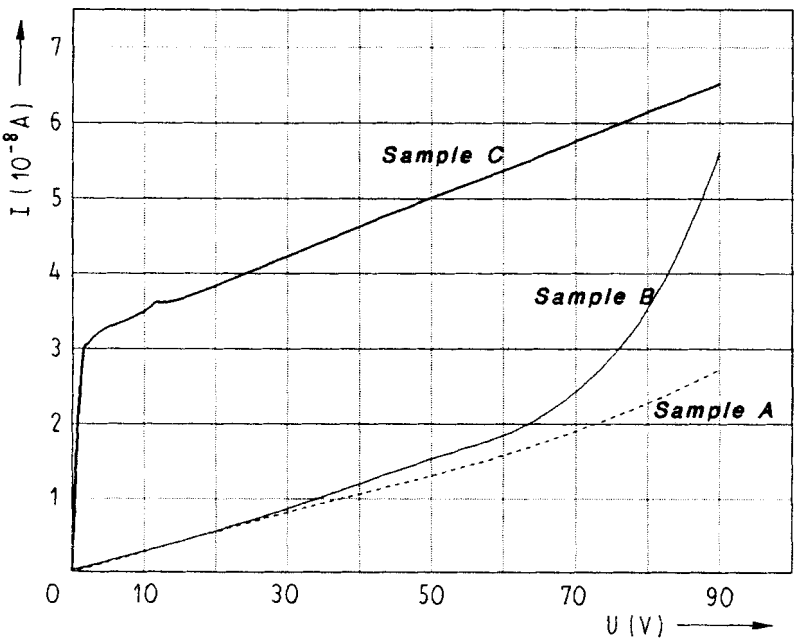

Fig. 1. Experimental $I-U$ curves for samples A, B, and C

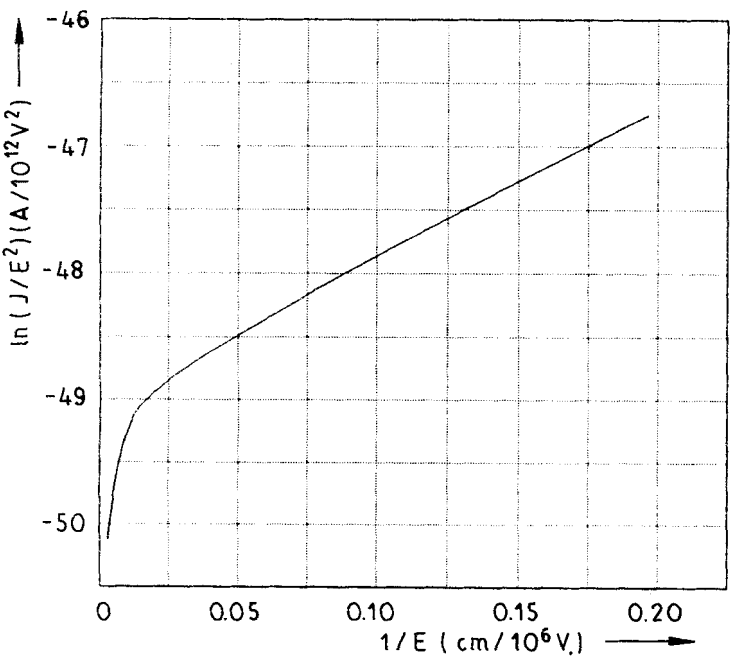

Fig. 2. Experimental $\ln(J/E^2) - (1/E)$ plot for sample A

this field E_i, the electron and hole conduction in the SiO_2 are small. From the $\ln(J/E^2)$ versus $1/E$ plot in Fig. 2, it is seen that the tunneling effect is not the dominant current conduction mechanism. Schottky emission, Frenkel-Poole emission, tunnel or field emission, space-charge limited, Ohmic and ionic conduction are the basic current conduction processes in insulators. For a given insulator, each conduction process may dominate in certain voltage ranges. The processes are also not exactly independent of one another and need to be carefully examined. A change of slope in the $\ln(J/E^2)$ versus $1/E$ plot is generally a reflection of the presence of conduction mechanisms other than tunneling.

5.3 High-frequency capacitance analysis

The high-frequency capacitance–voltage technique was used to investigate the effects of any contamination incorporated in the oxide. For these measurements, a micromanipulator $C-U$ system has been used. It consist of a model 410 $C-U$ plotter, Model HSM, temperature controller, and a S5/S6 test station.

In Fig. 3, an illustrative $C-U$ curve is presented in order to explain the different stages of $C-U$ analysis. The representative experimental $C-U$ curves are presented in Fig. 4. Each set of curves consists of a forward direction (accumulation to depletion swept $C-U$ curve and a reverse direction (inversion to accumulation) curve. The $C-U$ software allows to display the forward and the reverse curve or both at a time. The sweep (ramp) rate is set at 100 mV/s for the measurement. During the forward curve, under normal conditions, the capacitor is driven into deep depletion as opposed to inversion (the sample should be shielded from light). After the forward curve is acquired, the sample is momentarily exposed to light. After a pause, the reverse curve sweeps from 1 MHz inversion through depletion to accumulation. From both the forward and reverse $C-U$ curves, as shown in Fig. 3 and 4, any hysteresis effects can be readily seen. The capacitance is measured by means of a 1 mV signal at 1 MHz. The resultant current is sensed with a current amplifier and phase-locked detector.

These measurements are taken by considering the following constants for the material and device:

diameter of circular dot (device) = 125 μm,
gate work function (Au) = 5 eV,
energy gap (InP) = 1.34 eV (at 300 K),
dielectric constant (InP) = 12.4,
electron affinity (InP) = 4.41 eV,
work function difference = 0.566 eV,
intrinsic carrier concentration = 1.2×10^8 cm^{-3},
Schottky factor = 1/2 (energy band) = 0.67 eV,
$\sqrt{N_c N_v} = \sqrt{4.5 \times 10^{17} \times 7 \times 10^{18}}$ cm^{-3},
doping concentration (sulfur) = 2×10^{19} cm^{-3}.

In this analysis, the ramp rate of the gate voltage was varied from 50 to 250 mV/s in steps of 50 mV/s and the $C-U$ parameters were measured. In the case of the $\ln(J/E^2)-1/E$ plot, shown in Fig. 2, the plot does not give a straight line. It is necessary to adopt a thick oxide behavior due to which it seems that the transmission of charge through the insulating layer cannot be solely due to simple tunneling. Some other process must also be involved such as ionic conduction or space-charge limited current resulting from carriers injected into the insulator.

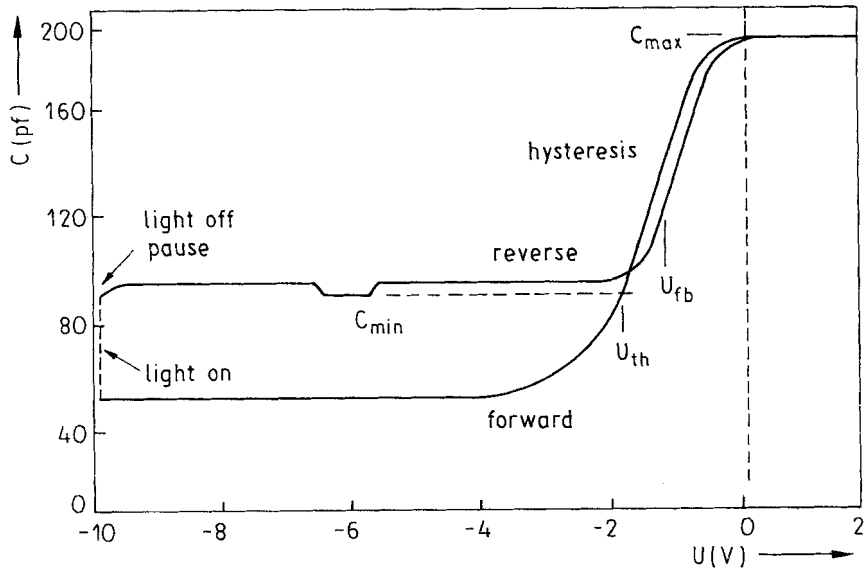

Fig. 3. C–U curve illustrating different stages of C–U analysis

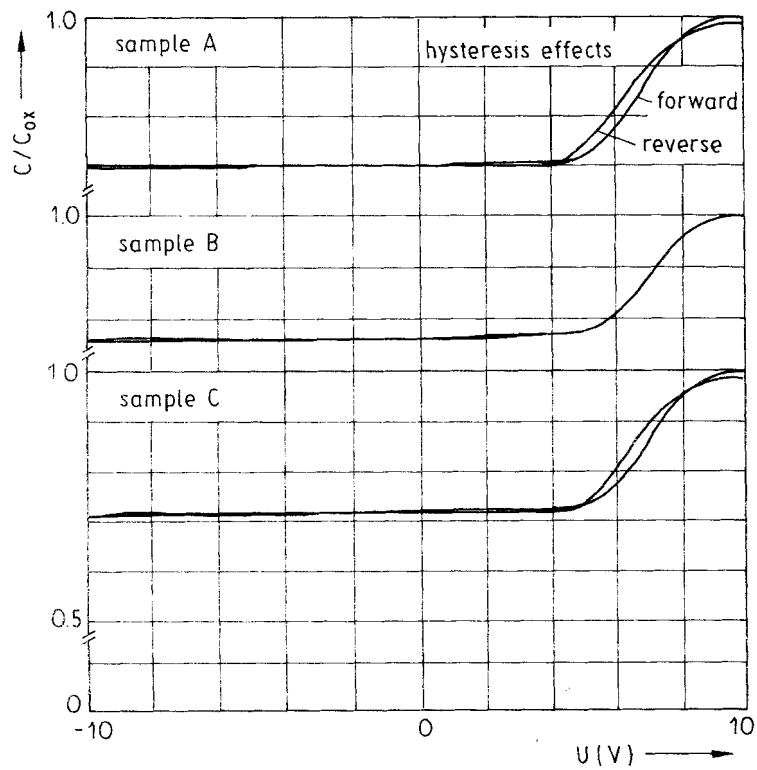

Fig. 4. Experimental C–U curves for samples A, B, and C

Table 1
Experimental results

sample	U_{th} (V)	U_{fb} (V)	N_{fix}*) (10^{11} cm^{-2})	t_{ox} (nm)	φ_B (V)	w_{max} (μm)
A	8.5	8.1	7.38	189	0.478	0.265
B	8.6	7.9	3.91	412	0.434	0.481
C	8.8	7.8	2.71	603	0.418	0.789

*) N_{fix} calculated using (6).

The trend noticeable from Table 1 is the decrease in φ_B with increasing oxide thickness t_{ox}. Using (5) for barrier heights in the semiconductor, the values of φ_B are seen to be within experimental range. The barrier height is a decreasing function of the oxide thickness t_{ox}, suggesting that current flow through the layer is not due to tunneling mechanism.

The FNT component of the $I-U$ characteristic is a function of the oxide thickness. Experimental $I-U$ curves for samples A, B, and C are reproducible as the applied voltage is not sufficient to cause destructive breakdown. In these experiments, the current is maintained at 1 μA to permit self-healing breakdwon. The $I-U$ characteristic obtained is then normalized by plotting $J-E$ plots, where J is the current density and E the field across the oxide, as shown in Fig. 5, so that we can compare all three samples A, B, and C. The

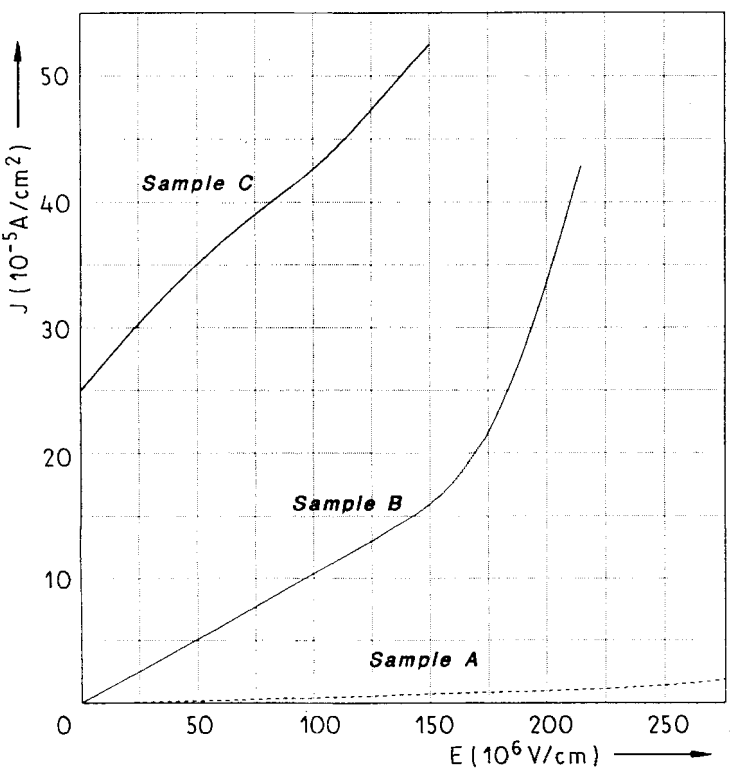

Fig. 5. Current density J vs. electric field E for samples A, B, and C

characteristics obtained for sample A shows increased carrier conduction around 150 MV/cm, for sample B it occurs at about 165 MV/cm while in case of sample C, this does not occur at least until 150 MV/cm. This is due to the increase in oxide thickness from A to C. The increased carrier conduction is reflected by a change in slope of the $J-E$ characteristics.

The $C-U$ curves indicated deviation from the ideal $C-U$ plot as reflected by the hysteresis. These shifts in $C-U$ curves in samples A and C, as shown in Fig. 4, are due to the nonzero φ_{ms}, nonzero U_{fb}, fixed oxide charge Q_{fix}, interface traps D_{it}, mobile ions, radiation effects, etc. In the case of sample B, we cannot see any hysteresis. In the present work, sweep rate is 100 mV/s and this rate is small enough that the $C-U$ curve does not exhibit deep depletion. The $C-U$ parameters obtained from computer simulation are tabulated in Table 1. As can be seen in the table, the obtained values of t_{ox} are in good agreement with measured values.

6. Conclusions

$C-U$ and $I-U$ measurements have been performed on MIS devices fabricated on InP substrates. The analysis of these measurements shows that tunneling is not the only current conduction mechanism in these devices. The $C-U$ measurements yield oxide thickness that are in accord with experimental data.

Acknowledgements

We are thankful to Dr. A. Katz of AT&T Bell Labs for supplying us the samples. The metallization was performed by Dr. D. Shah at Bellcore. The financial support of the New Jersey Commission of Science & Technology and the Center for Manufacturing Systems is gratefully acknowledged.

References

[1] C. J. HUANG and Y. K. SU, J. appl. Phys. **67**, 3350 (1990).
[2] O. WADA and A. MAJERFELD, Solid State Electronics **25**, 381 (1982).
[3] H. LIM, G. SAGNES, and G. BASTIDE, J. appl. Phys. **53**, 7450 (1982).
[4] M. S. PATEL, MS Thesis, New Jersey Inst. Technology, Newark(NJ) 1991.
[5] R. J. ARCHER, J. Opt. Amer. **52**, 970 (1962).
[6] D. K. SCHRODER, Advanced MOS Devices, Modular Series on Solid State Devices, Addison-Wesely Publ. Co., Reading (Mass.) 1988.
[7] $C-V$ Operator Manual, Micromanipulator Co., Inc., Carson City (Nev.) 1988.
[8] E. HARARI, J. appl. Phys. **49**, 2478 (1978).

(Received March 30, 1992; in revised form June 29, 1992)